3D printing of self-standing and vascular supportive multi-material hydrogel structures for organ engineering

Qingxi Hu[1], Suihong Liu[1], Haiguang Zhang[1], Zhipeng Shen[1], Sasirekha Krishnan[2], and Murugan Ramalingam[3]

[1]Shanghai University
[2]VIT
[3]Centre for Stem Cell Research

June 7, 2021

Abstract

Three dimensional printable formulation of self-standing and vascular-supportive structures using multi-materials suitable for organ engineering is of great importance and highly challengeable, but, it could advance the 3D printing scenario from printable shape to functional unit of human body. In this study, the authors report a 3D printable formulation of such self-standing and vascular-supportive structures using an in-house formulated multi-material combination of albumen/alginate/gelatin (A-SA-Gel)-based hydrogel. The rheological properties and relaxation behavior of hydrogels were analyzed prior to the printing process. The suitability of the hydrogel in 3D printing of various customizable and self-standing structures, including a human ear model, was examined by extrusion-based 3D printing. The structural, mechanical, and physicochemical properties of the printed scaffolds were studied systematically. Results supported the 3D printability of the formulated hydrogel with self-standing structures, which are customizable to a specific need. In vitro cell experiment showed that the formulated hydrogel has excellent biocompatibility and vascular supportive behavior with the extent of endothelial sprout formation when tested with human umbilical vein endothelial cells. In conclusion, the present study demonstrated the suitability of the extrusion-based 3D printing technique for manufacturing complex shapes and structures using multi-materials with high fidelity, which have great potential in organ engineering.

3D printing of self-standing and vascular supportive multi-material hydrogel structures for organ engineering

Qingxi Hu[1,2,3], Suihong Liu[1], Haiguang Zhang[1,2,3,*], Zhipeng Shen[1],Sasirekha Krishnan[4], Murugan Ramalingam[4,*]

[1]*Rapid Manufacturing Engineering Center, Shanghai University, Shanghai 200444, China*

[2]*Shanghai Key Laboratory of Intelligent Manufacturing and Robotics, Shanghai University, Shanghai 200072, China*

[3]*National Demonstration Center for Experimental Engineering Training Education, Shanghai University, Shanghai 200444, China*

[4]*Biomaterials and Organ Engineering Lab, Centre for Biomaterials, Cellular and Molecular Theranostics, School of Mechanical Engineering,Vellore Institute of Technology, Vellore 632014, India*

[*]*Author for correspondence:*

Prof. Haiguang Zhang: E-mail address: haiguang_zhang@i.shu.edu.cn

Prof. Murugan Ramalingam: E-mail address: rmurug2000@gmail.com

Abstract

Three dimensional printable formulation of self-standing and vascular-supportive structures using multi-materials suitable for organ engineering is of great importance and highly challengeable, but, it could advance the 3D printing scenario from printable shape to functional unit of human body. In this study, the authors report a 3D printable formulation of such self-standing and vascular-supportive structures using an in-house formulated multi-material combination of albumen/alginate/gelatin (A-SA-Gel)-based hydrogel. The rheological properties and relaxation behavior of hydrogels were analyzed prior to the printing process. The suitability of the hydrogel in 3D printing of various customizable and self-standing structures, including a human ear model, was examined by extrusion-based 3D printing. The structural, mechanical, and physicochemical properties of the printed scaffolds were studied systematically. Results supported the 3D printability of the formulated hydrogel with self-standing structures, which are customizable to a specific need. *In vitro*cell experiment showed that the formulated hydrogel has excellent biocompatibility and vascular supportive behavior with the extent of endothelial sprout formation when tested with human umbilical vein endothelial cells. In conclusion, the present study demonstrated the suitability of the extrusion-based 3D printing technique for manufacturing complex shapes and structures using multi-materials with high fidelity, which have great potential in organ engineering.

Keywords: Multi-material hydrogel; extrusion-based 3D printing; self-standing structures; endothelial sprouting; organ engineering.**1. Introduction**

The recent advances in 3D printing alias additive manufacturing technology opens tremendous possibilities of engineering tissues and organs, which mimic native structure and function to some extent. The emerging 3D printing technology enables even to fabricate anatomy-specific 3D shapes and structures suitable for organ engineering[1] [2]. Although rapid progress has been witnessed in the past decade, there are limitations to the existing printing technology. For instance, conventional 3D printing often employs bioinks made up of single-phase biomaterial, which may not be sufficient to construct precise biomimetic architecture. Therefore, there is a need to develop a 3D printing technology that utilize printing of multiple biomaterials to construct a complex tissue architecture that could accommodate various cell types and biomolecules, required for emulating physiologically relevant tissues or organs.

Biomimetic approach in 3D bioprinting often requires self-standing and vascular supportive multi-material bioinks to realize the translational potential of 3D bioprinting towards clinical applications, from bench to bedside. Atabak et al., proposed a method to develop alginate-based self-supportive scaffolds for creating tubular structures and employed a crosslinking strategy to strengthen the scaffolds [3]. However, the application of this strategy was limited by the crosslinking agents and the precise regulation of degree of crosslinking in each step. Alternatively, thermosensitive and photoactivated materials were applied to improve the printability of large-size tissue-engineering structures. The self-supporting properties of the thermo-/photo- activated materials, such as gelatin, poly(ethylene glycol), and gelatin methacryloyl, were improved by controlling the temperature or light at the extrusion nozzle exit to modulate the bioink's pre-crosslinking, but, this strategy is limited by its versatility, such as the accurate control over the degree of crosslinking and availability of thermo-/photo- activated materials [4]. Bin et al. utilized the alginate/gelatin-based multi-material hydrogel formulation to improve the printing accuracy and biomechanics of printed structures; heterogeneous aortic valve conduits, for example [5]. Alexandra et al., demonstrated a multi-material bioink-based printing method using polyethylene glycol crosslinking for expanding the biomaterial palette required for bioprinting of customizable tissue and organ scaffolds [6]. The printed scaffolds facilitated high cell viability during the course of the study. To obtain a mechanically and biologically enhanced cell-laden structure, Yeo et al., employed a coaxial extrusion printing method using collagen-based bioink (core) and pure alginate-based bioink (shell) to prepare cell-laden mesh structure [7]. The fabricated cell-laden 3D core-shell structure exhibited excellent cell viability and efficient hepatogenic differentiation were observed. All these experimental studies, and others, were clearly demonstrated the efficacy of multi-material formulation strategy and it's potential in creating complex shapes and structures suitable for tissue or organ engineering.

Among others, vascularization is one of the essential factors for organ engineering and therefore, the biomaterials that are used for 3D printing should have the ability to support and promote sufficient neovascularization within the engineered tissue and organ. Several studies reported different strategies to facilitate vascularization within the bioengineered constructs, including growth factor and co-culture strategy [8, 9]. The growth factor strategy often causes atherosclerosis and abnormal blood vessels because the amount of growth factors cannot be precisely controlled [10]. The co-culturing of different cells, such as endothelial cells, adipose stem cells, mesenchymal stem cells, *etc.* were commonly used to study the self-promoted vascularization [11]. However, high operational difficulty, low cell viability, and high-cost are some of the common factors that greatly influence the effectiveness of this method.

In a previous study, the authors were inspired by the processes of chicken eggs hatching; lots of angiogenesis were formed in egg white, transfer nutrition in egg white to embryo. Then authors reported the 3D printing ability of a novel multi-material formulation, based on albumen (egg white) and alginate, to promote angiogenic sprouting and vascular network formation [12]. Though the albumen/alginate-based hydrogel formulation has excellent 3D printability, it has its own limitations and challenges in printing large-scale structures. The present research is therefore intended to improve the efficiency of the albumin-rich hydrogel formulation with unique combination of A-SA-Gel, having self-standing and vascular-supportive properties suitable of engineering complex shapes and structures with high fidelity.

2. Materials and method

2.1 Materials

The raw materials required to conduct the experiments are mentioned as follows. The chicken eggs were purchased from a local farm less than 7 days after laying. The surface of the egg was washed in deionized water and sterilized in ethanol (75%). Then, egg white (EW) was separated from the yolk, also called as albumin, and used in the preparation of hydrogels without any further treatment. Sodium alginate (SA), calcium chloride ($CaCl_2$) and gelatin (Gel) (type A from porcine skin, 300 blooms) were purchased from Sigma-Aldrich (USA) and used in same condition as received. The HUVECs were obtained from Zhongqiaoxinzhou Biotech (China).

2.2 Formulation of A-SA-Gel hydrogel

According to previous research [12], first, the 5% (w/v) SA and 10% (w/v) Gel solution was made in deionized water followed by mixing both of them at the volume ratio of 1:1. Secondly, the albumin was added and gently mixed with the SA/Gel solution at the volume ratio of 1:5 in order to get the A-SA-Gel hydrogel. Finally, the hydrogel was stirred constantly until free from air bubbles and stored in refrigerator (4-10) for further use.

2.3 Rheology of A-SA-Gel hydrogel

The rheological properties of the A-SA-Gel hydrogel were analyzed by using a rotational rheometer (DHR-3, TA Instruments, USA). A cone plate geometry was adopted according to the manufacturer's protocol, in which the diameter and interpolate gap were 30 and 1 mm, respectively. The steady-shear rate sweeps were conducted on the hydrogel sample, which was carefully loaded onto the plate fixture without the air bubbles at room temperature. Before performing the shear test, all samples were held for 15 min to eliminate thermal and shear histories. The storage and loss modulus of the hydrogel samples were measured as a function of strain amplitude sweep test and frequency.

2.4 3D printing of A-SA-Gel hydrogel scaffolds

To fabricate the A-SA-Gel hydrogel scaffolds, an in-house built extrusion-based 3D printing system was employed. The schematic representation of the material preparation and printing process is shown in Figure 1A. The system and solution parameters were optimized prior to 3D printing. Briefly, the printing system was designed with a computer controlled automated X–Y–Z stage, a receiving platform, a nozzle mounting block, a printer head (syringe needle), and a pneumatic (pressured-air) system, which consist of compressor,

air tube, and control valve. The syringe needle was directly connected with the pneumatic system through air tubes. The pneumatic controller provided air pressure for extruding hydrogel material. The receiving platform was mounted in the X-Y plane that was capable of printing with high precision; the syringe needle mounted to a solo motorized linear Z-axis, and it can be controlled to move up and down. The prepared A-SA-Gel hydrogel was gently added to a 50 ml syringe, and a 22G needle was used for extrusion printing.

In order to print a grid-structured scaffold, as a model scaffolding system, having the size 20 ×20 × 5 mm (L×W×H), and the following parameters were used. The interval of parallel-arranged filaments within the grid structure was kept 0.6 ± 0.1 mm in each layer, and adjacent layers were perpendicularly stacked to construct the porous structure. During the printing process, the prepared A-SA-Gel hydrogel was extruded from the syringe needle to generate continuous filament at room temperature, and the extruded filaments deposited layer-by-layer to form the grid-structured A-SA-Gel hydrogel. A stable air pressure value of 2.8 ± 0.1 Psi was applied to extrude hydrogel. After printing, the hydrogel was crosslinked with $CaCl_2$ solution (4%, w/v), followed by oven-dried for 3 h at 37 °C.

In addition, a thick scaffold structure (10(L)×10(W)×10(H) mm), blood vessel structure (12mm in diameter, 15mm in height), the abbreviations of Shanghai University (SHU) and Vellore Institute of Technology (VIT), and human ear models were also printed under the optimal conditions, in order to further evaluate the 3D printability and self-standing ability of the A-SA-Gel hydrogel, in terms of various shapes, sizes and structures.

2.5 Characterization of the A-SA-Gel hydrogel scaffolds

2. 5.1 Morphological analysis

The morphology of the various A-SA-Gel hydrogel printed samples was examined by using a scanning electron microscope (SEM, HITACHI SU-1510, Japan). All the samples were coated with gold for 120 seconds using a gold sputter coater and then the surface and cross-sectional views were analyzed under at an accelerating voltage of 10 kV.

2.5.2 Chemical functional group analysis

In order to analyze the characteristic functional groups of the raw materials such as albumen, SA, gelatin, and the formulated A-SA-Gel hydrogel, Fourier transform infrared spectroscopy (FTIR) technique was employed using a Thermo Nicolet AVATAR 370 spectrometer. The spectra were recorded over the wave number range of 4000–800 cm^{-1} and the data were analyzed.

2.5.3 Swelling kinetics study

The swelling behavior of the control SA/Gel as well as the fabricated A-SA-Gel hydrogel samples was analyzed by immersing the samples in Roswell Park Memorial Institute (RPMI) 1640 culture medium and phosphate buffered saline (PBS) at pH 7.4 at 37 °C for 3 h. The swelling percent (%) was calculated according to the following equation:

$$\text{Swelling } (\%) = [(W_t - W_o)/ W_o] \times 100\%$$

For which, the samples were dried at 37 °C and the dry weight (W_o) of the same was captured. Then, the samples were immersed in culture medium and PBS. The swollen weight (W_t) of the samples was measured every 15 min after removing excess solution from the surface of the samples with lint-free filter paper, until no further change in weight. All samples were analyzed in triplicate.

2.5.4 Drying kinetics study

The drying kinetics of the control SA/Gel as well as the fabricated A-SA-Gel hydrogel samples was investigated by weighing their weight loss at predetermined time intervals. In order to measure the drying kinetics and water content of the A-SA-Gel hydrogel, three samples were fabricated and dried at 37 °C. The dry weight (W_o) of samples were recorded. Then, the samples were immersed into PBS solution for 2 h at 37 °C, and the swollen weight (W_m) of samples was captured. Finally, the swollen samples were dried at 37 °C

and the dry weight (W_t) was measured every 15 min until no further change in the weight of the samples. The drying percent (%) was calculated according to the following equation:

Drying (%) = $[(W_t - W_o) / (W_m - W_o)] \times 100\%$

2.5.5 Degradation study

The degradation behavior of the control SA/Gel and A-SA-Gel hydrogel samples was examined by immersing them in SBF at pH 7.4 at 37 °C, simulating the degradation condition by hydrolysis. In this study, the samples were weighed (dry mass M_o) and placed into a petri dish with PBS (pH 7.4) and RPMI 1640 culture medium, separately. The samples were incubated at 37 °C for up to 5 days, and PBS and culture medium were replaced every day. After the predetermined time intervals, the samples were wrapped with lint-free filter paper to remove excess PBS or culture medium from the surface of the samples and then kept into a drying oven at 37 °C to dry. The final mass of dry samples was recorded (M_t). The percentage of weight loss was calculated according to the following formula:

Weight loss (%) = $[|M_t - M_o|/ M_o] \times 100\%$

The morphology of the SA/Gel and A-SA-Gel hydrogel samples were also examined by using SEM (HITACHI SU-1510, Japan) after degradation of 1, 3 and 5 days.

2.5.6 Mechanical properties

A uniaxial testing method was conducted to test the mechanical properties of the SA/Gel and A-SA-Gel hydrogel samples. The compressive strength was determined with a WDW-1 universal testing machine with a constant compression speed of 0.2 mm/min at room temperature. The testing dimensions of the samples were of 20 ± 0.5 mm × 20 ± 0.5 mm × 6 ± 0.25 mm. Each experiment was performed in triplicate. The stress-train curve of the samples were measured and plotted. In addition, the tensile strength of SA/Gel and A-SA-Gel hydrogel samples were also tested according to the manufacturer's instructions.

2.6 Cell culture study

The HUVECs were cultured as per the manufacturer's procedure in RPMI 1640 cell culture medium, which consisted of 10% fetal bovine serum, 0.292 mg/mL L-glutamine, 4.766 mg/mL HEPES, 0.85 mg/mL $NaHCO_3$, 1% penicillin (100 units/mL), and streptomycin (100 µg/mL). The cells were maintained at 37 °C in a humid atmosphere containing 5% CO_2. The culture medium was replaced every day, after cultured for the first three days, and the cells then suspended in fresh medium. The final suspension density of 6×10^6 cells/mL was prepared. The samples of SA/Gel and A-SA-Gel hydrogel scaffolds were sterilized by 75% ethanol for 6 h under UV light and then rinsed three times with sterilized PBS. Next, the scaffolds were immersed in a fresh cell culture medium for 2 h before cell seeding. Finally, the cell suspension was lightly inoculated on the treated A-SA-Gel hydrogel scaffold until the surface of the scaffold was fully covered. After 4 h of initial cell attachment, the culture medium was added gently until the whole scaffolds were completely immersed. The experiments were conducted under static cell culture conditions and the cell culture medium was changed every day. Moreover, the prepared SA/Gel scaffold without albumen as a control group.

2.7 Cell characterization

The viability of cells cultured on the SA/Gel and A-SA-Gel hydrogel samples was tested by Live/Dead staining assay (Biovision Inc., USA) according to the manufacturer's recommendations, after 4 days of culture. The assay kit contains Calcein-AM, a cell-permeable green fluorescent dye (Ex = 490nm, Em = 515nm), to stain live cells, while the dead cells were stained by red fluorescent dye called propidium iodide (PI). Briefly, the staining assay was prepared using a mixture of 1 µL of Calcein-AM and 5µL of PI in 1 mL of staining buffer according to the manufacture's protocol. The samples were removed from the culture medium after culturing 4 days and gently washed with PBS. Then, the prepared staining assay was added directly to the samples and incubated for 15 min at 37 °C. The stained samples were mounted on a microscope slide for imaging under an inverse fluorescence microscope (Eclipse Ti-U, Nikon Instruments Inc. Japan).

In addition, the HUVECs culture on the SA/Gel and A-SA-Gel hydrogel samples were stained with 4',6-diamidino-2-phenylindole (DAPI) and tetramethylrhodamine (TRITC) phalloidin to visualize the cell nucleus and cytoskeleton, respectively. Briefly, the cell cultured samples were rinsed 3 times in PBS, fixed in situ with 4% paraformaldehyde for 10 min, permeabilized with 0.5% Triton X-100 for 5 min. Then, 100 μL of TRITC-phalloidin was gently added to the samples until it covers completely, and then it was incubated in a dark environment for 30 min at room temperature to stain the cell cytoskeleton. After that, the samples were washed 3 times in PBS, and 100μL of DAPI solution was added to the samples for 30 s to stain the cell nucleus. The fluorescence images were captured by a fluorescence microscope. Moreover, the cell adhesion morphology on the surface of the A-SA-Gel hydrogel samples was observed by using SEM after culturing for 4 days. Briefly, the cell-laden scaffolds were removed from the culture medium and gently washed with PBS, then immediately fixed with 4% paraformaldehyde for 1h, and washed with PBS three times. After that, the samples were immersed in different concentrations of ethanol (25%, 50%, 75%, 85%, 95%, and 100%) for 5 min for dehydration. The samples were then immersed in the mixed solutions of the absolute ethyl alcohol and hexamethyl disilylamine (3:1, 1:1, 1:3, and 0:1) for 10 min, followed by sputter coating with gold before imaging.

The quantitative analysis of the cell viability/proliferation was performed using Cell Counting Kit-8 (CCK-8) assay. CCK-8 allows sensitive colorimetric assay for the determination of the number of viable cells. Briefly, the SA/Gel and A-SA-Gel hydrogel samples were sterilized by 75% ethanol and added to a standard Petri dish (Corning, NY) with fresh culture medium for 2 h under the UV light. Then, the samples were added to the wells of 96-well plates (50 μL per well, Corning, USA). The prepared cells suspension was added into each well with printed samples at the density of 1×10^5 cells/mL. Three rows of the well of each plate were covered in every group. The cells were incubated at 37 °C in a humid atmosphere with 5% CO_2. After 1, 3, and 5 days of incubation, 10μL of CCK-8 solution was injected into each well and incubated for 2 h in a CO_2 incubator at 37 °C. The absorbance of 450 nm was determined by using a microplate reader (Infinite 200Pro, Tecan Group Ltd., Switzerland). The SA/Gel hydrogel sample was also tested as a control group. In addition, the cells suspension without a sample as a positive control group and only contain CCK-8 and medium as a background group.

2.8 Statistical analyses

The data acquired in this study are represented as means ± standard deviation (SD). The one-way analysis of variance (ANOVA) is used to determine the statistical differences with Origin 2017 software and a p -value < 0.05 was considered statistically significant.

3. Results

3.1 Rheological Testing of A-SA-Gel hydrogel

Viscoelasticity is one of the key features that determines the ability of a biomaterial to be suitable for 3D printing application. The viscoelastic properties of the A-SA-Gel hydrogel are shown in Figure 2A, which represents its shear thinning behavior. The results of steady-shear rate sweeps are plotted in Figure 2B, which shows higher storage modulus and lower loss modulus of the crosslinked hydrogel. It is one of the highly required behaviors of any biomaterial to be 3D printed into various structures with high fidelity.

3.2 3D printing of A-SA-Gel hydrogel scaffolds

The A-SA-Gel hydrogel scaffolds were fabricated by extrusion-based 3D printing technique followed by crosslinking under the optimal conditions as described previously. The scaffolds were printed with eight layers, having the final size of 20 × 20 × 5 mm (L×W×H). A representative gross view of the as-printed scaffold is presented in Figure 2C and top-angle view of the same is shown in Figure 2D. The scaffold was printed as per the pre-designed architecture without any deformation.

3.3 Morphological analysis

The SEM micrographs of a representative 3D printed A-SA-Gel hydrogel scaffolds are shown in Figure

2E-2M, where surface and cross-sectional morphologies of the scaffolds and filament structural features were investigated. It was found that the mesh-like structural features were obvious and they are structurally intact well. In addition, the SEM analysis revealed the porous nature of the printed scaffolds with rectangular architecture (Figure 2E-2F). It is noteworthy that the intersections of adjacent layers of filaments were tightly intact and connected (Figure 2G). In addition, the filaments of different layers were aligned, and the interlayer structure is clearly visible (Figure 2H-2I). The uneven rough surface morphology was observed (Figure 2J). The surface morphology of single filament was also analyzed and the results are shown in Figure 2K-2M. The wavy micro rough surfaces were noticed from the high-resolution images of the scaffold. The average diameter of the filament was found to be 385μm, which is distinctly smaller than the 22G nozzle's inner diameter of 410μm.

To further verify the printability and self-standing ability of the A-SA-Gel hydrogel suitable to use as a scaffolding system, various structures were printed out as a model and the results are presented in Figure 3. A thick cube scaffold structure is shown Figure 3A. A blood vessel structure can be seen from Figure 3B. The abbreviations of Shanghai University (SHU) and Vellore Institute of Technology (VIT) were printed out as pictured in Figure 3C. Importantly, human ear-like structures were also fabricated without any noticeable deformation and the results are presented in Figure 3D. All these are the experimental examples serve as a proof that the multi-material hydrogel developed in this study can be utilized for 3D printing of various structures and shapes with high fidelity.

3.4 Chemical functional group analysis

The chemical functional groups of the SA, albumen, Gel, and A-SA-Gel samples were studied by FTIR spectroscopy and the results are depicted in Figure 4A. As seen from the FTIR spectra, the characteristic peaks of SA appear at 1610, 1416, and 1042 cm^{-1}. The characteristic peaks of albumen appear at 1621, 1536, and 1251 cm^{-1}. For the Gel sample, the characteristic peaks were 1661, 1582, 1516, and 1252 cm^{-1}. As for as the A-SA-Gel hydrogel sample, the most prominent peaks are appeared at 1650, 1546, 1455, 1241, and 1021 cm^{-1} as seen from the spectrum

3.5 Swelling Analysis

The swelling data of the A-SA-Gel and SA/Gel hydrogel samples as a function of time in PBS and RPMI 1640 culture medium at 37 °C are presented in Figure 4B-4C. From the results, it was observed that the swelling ratios of the SA/Gel sample were higher than that of A-SA-Gel sample. It can also be seen from the graph that the similar results were observed for the study conducted in RPMI 1640 culture medium. The swelling ratio of the SA/Gel sample was about twice as high as that of the A-SA-Gel sample. There was a noticeable phenomenon that the swelling ratios of SA/Gel and A-SA-Gel samples increased fastest in the first 15 min, and stabilized after 30 min.

3.6 Drying Kinetics Analysis

Figure 4D shows the time-dependent drying kinetics of the prepared SA/Gel and A-SA-Gel hydrogel samples in the form of the (W_m - W_t) / (W_m - W_o) curves versus time, at drying temperature of 37°C. The drying curves showed that the drying ratio of all of groups increased with the increase of time, and become to steady state after 130 min. The drying ratio of the SA/Gel sample was faster than that of the A-SA-Gel sample. For example, the fraction of water removed from the SA/Gel sample during the first 15 min of drying period was 35.22%, while this fraction for the A-SA-Gel sample was 26.06%.

3.7 Degradation Analysis

The degradation data of SA/Gel and A-SA-Gel samples were obtained from the experiments conducted in RPMI 1640 culture medium at 37 °C is presented in Figure 5. To investigate further on how the degradation influences the microstructural features of the samples, the morphological analysis was carried out for the SA/Gel and A-SA-Gel samples after the degradation study conducted in RPMI 1640 culture medium for 1, 3 and 5 days. The SEM micrographs of A-SA-Gel (Figure 5 A-A2) and SA/Gel (Figure 5 B-B2) samples showed that they lose their structural integrity and the scaffolds look fluffy over time period. The degradation

behavior of SA/Gel and A-SA-Gel samples in culture medium shown in Figure 5C indicated that the degree of dissolution increased over the time period during the course of study. It was also noticed that the degree of dissolution of A-SA-Gel sample was higher than that of SA/Gel sample. It can be seen from the graph that nearly 50% of the A-SA-Gel sample is solved in the first three days, and then the rate of dissolution slowed down after five days. The similar results were observed for the same samples but the experiments conducted in PBS (Figure 5D). There was a noticeable difference that the degradation of the A-SA-Gel sample in PBS was higher than in the culture medium after 5 days (Figure 5E).

3.8 Mechanical Properties

The mechanical properties, in particular compressive and tensile strength, are of great importance for the scaffolds that are to be used in tissue or organ engineering applications, especially when dealing with load-bearing structures. The compression and tension tests of the 3D printed SA/Gel and A-SA-Gel hydrogel scaffolds. The stress-strain curve is shown in Figure 6. Interestingly, the strain of A-SA-Gel hydrogel scaffold was higher than that of the SA/Gel scaffold. Moreover, the compressive strength of A-SA-Gel hydrogel scaffold exceeded 6 MPa, and the strain of A-SA-Gel hydrogel scaffold more than 55% (Figure 6, left panel). As for the tensile strength, the stress and strain of A-SA-Gel hydrogel scaffold were higher than that of SA/Gel scaffold (Figure 6, right panel). The maximum value of tensile stress in A-SA-Gel hydrogel scaffold was 0.221 MPa, while the SA/Gel scaffold was found to be 0.184 MPa. Also, the maximum strain of the A-SA-Gel hydrogel scaffold was found to be more than 450 %, which was higher than the A-SA-Gel hydrogel substrate.

3.9 In *Vitro* Cell Studies

To evaluate the cell compatibility and vascular potential of the 3D printed A-SA-Gel hydrogel scaffold, HUVECs were cultured as a model cell type. The SA/Gel hydrogel scaffold served as a control group. The morphology of cultured cells and detection of live/dead cells were performed to analyze the viability of HUVECs in 3D printed constructs after 4 days of culture (Figure 7). The microscopic images of cultured cells (Figure 7A, 7D, and 7G) showed that the cells were evenly distributed and adhered well to the scaffolds. The cells were maintained their normal cellular phenotypes. The cell density of the A-SA-Gel hydrogel scaffold (Figure 7D) was higher than that of SA/Gel scaffold (Figure 7A). The live/dead cell staining images showed that the majority of HUVECs in all groups were stained green (Figure 7B, 7E, and 7H), indicating the high cellular viability. However, there few dead cells were also observed (Figure 7C, 7F, and 7I). Importantly, the endothelial sprout formation and primitive microvascular networks were observed for the A-SA-Gel hydrogel scaffold (Figure 7E and 7H) as compared to the SA/Gel scaffold (Figure 7B). To this end, more representative fluorescence images of endothelial sprouts, vessel networks, and neovessels were captured at different A-SA-Gel hydrogel scaffold areas, as shown in Figure 8, at higher magnification. The endothelial vascular network formation due to endothelial cellular function was captured in Figure 8A, along with lacunae (micro-rings) microstructures within the network. The diameter of the lacunae (micro-rings) of endothelial network was measured (Figure 8G), and the average was found to be 31.25$\pm$0.58μm. Figure 8B presented a microvessel of endothelial cells like a bridge, interconnected between adjacent sides. Exhilaratingly, a branched microvessel network was observed like a tree branch in Figure 8C. Moreover, several large neovessels with obvious open lumen were captured in Figure 8D-8F, and the average diameter was more than 100μm. To further analyze vasculogenesis, the diameter of endothelial sprouting and sprouting length was measured (Figure 8H and 8I). The minimum diameter of endothelial sprouting was 8μm, and the maximum diameter was about 112μm. For the sprouting length, the minimum sprouting length was 118μm, the maximum length was 476μm, and the average length was 289 μm.

Additionally, fluorescent staining of the cell-cultured A-SA-Gel hydrogel scaffold was carried out to visualize the cell nucleus and cytoskeleton after 4 days of culturing (Figure 9A-A2, 9B-B2, and 9C-C2). A homogeneous distribution of cells on the surface of the scaffold was observed in the DAPI (cell nucleus) and TRITC-phalloidin (cytoskeleton) stained images (Figure 9 A-A2). Similarly, the representative fluorescence images of the endothelial sprouts and neovessels were also presented (Figure 9B-B2 and 9C-C2). Moreover, the SEM photographs of HUVECs on the scaffold were shown in Figure 9D-9F. The SEM examination of the cells

confirmed good attachment and spreading of cells on the surface of the scaffold. These cells were observed to be flat-shaped and stretch on the whole surface of scaffold structures.

3.10 CCK-8 Assay

In order to evaluate the proliferation of HUVECs cultured onto A-SA-Gel and SA/Gel hydrogel scaffolds, CCK-8 assay test was performed on day 1, 3, and 5 after cell culture and the obtained data is shown in Figure 9G. It was demonstrated that, compared with day 1, the OD values at a wavelength of 450 nm increased by around 2 times in all groups after culturing for 3 days. The cell growth in all groups was seen to be sharply improved on day 5, and the OD values of the A-SA-Gel group increased by about 6 times than that of day 1. Moreover, the OD values of the A-SA-Gel group even more than the control and SA/Gel groups. These results indicated that the cells can maintain their proliferation ability when cultured with the fabricated A-SA-Gel hydrogel scaffolds. Due to their favorable characteristics, such as cell compatibility and non-toxicity, the 3D printed A-SA-Gel hydrogel scaffolding system may find application in various tissue or organ engineering.

4. Discussion

The identification and optimization of a suitable biomaterial that can have self-standing and vascular supportive properties are of great importance and are in demand for organ 3D printing. Though some of the single-phase biomaterials are being used in the preparation of bioinks, they often lack on the ability of accommodating multiple cell types suitable for organ engineering. Therefore, it is essential to develop multi-material-based bioinks in order to advance the field of 3D printing toward development of functional tissues and organs.

Keeping these points in view, in this study, a newly formulated multi-material hydrogel, based on the combination of A-SA-Gel, was developed and investigated their suitability in 3D printing of various simple and complex engineered shapes and structures applicable for tissue and organ engineering. As far as to our knowledge and through the literature surgery, this is the first study which explores the preparation and 3D printing of multi-material A-SA-Gel hydrogel using the combination of albumen, sodium alginate and gelatin.

Alginate is an anionic and hydrophilic polysaccharide derived from seaweeds. SA is one of the commonly used bioinks in 3D bioprinting due to its cell compatibility, and rapid and tunable gellation due to its excellent crosslinkability in the presence of ionic calcium solution or other divalent cations [13]. Although SA has excellent biocompatibility, it lacks bioactivity. Therefore, it is necessary to improve its bioactive functional properties suitable for engineering tissues and organs. Gelatin is a highly cell compatible and biologically active polymer derived from collagen by partial hydrolysis [14]. It is also widely used as a bioink either as such or in combination with other polymers, including alginate. The combination of alginate and gelatin often used as a bioink in 3D printing due to their enhanced functional properties as compared to their individual component. However, their ability of neovascularation is not satisfactory. In order to enhance their vascular supportive ability, the authors have introduced albumen, and its vascular supportive behavior has already been demonstrated in their earlier study [12]. In this study, a unique combination of albumin, SA, and gelatin has been developed in order to formulate a novel A-SA-Gel hydrogel to enhance their 3D printability, self-standability, and vascular supportivity of their individual component.

The A-SA-Gel hydrogel was prepared under optimized experimental conditions, and it was thoroughly characterized prior to printing. The current study employed an extrusion-based 3D printing. The hydrogel was subjected to 3D printing under various system and solution parameters in order to optimizing the conditions which could generate and extrude the continuous filaments, leading to various simple and complex engineered shapes and structures through layer-by-layer. As soon as the scaffolds were printed, they were cross-linked by means of chemical ions in order to further strengthen their structural and shape fidelity. The experimental conditions were optimized so that the scaffold's integrity could be intact and maintained for the initial days during the course of study. The printed scaffolds exhibited high fidelity and robustness.

The viscoelastic properties of the A-SA-Gel hydrogel exhibited shear thinning behavior (Figure 2A), similar to the other bioinks,such as cellulose nanofibers (CNFs) and methacrylated gelatin (GelMA) composite bioink[15] and vascular-tissue-derived decellularized extracellular matrix (VdECM) and alginate-based bioink[16], which favor excellent printability and viability of the entrapped cells due to the alleviated shear stress when passing through printing nozzles at a certain flow rate [17]. The shear stress sweep results showed low loss modulus and high storage modulus of the crosslinked hydrogel (Figure 2B), which further confirms the ability of the A-SA-Gel hydrogel to retain its shape and structure.

After the pre-printing optimization, the A-SA-Gel hydrogel was subjected to print in order to evaluate its printing ability and integrity of the printed structure and shape fidelity. The printer head needle with 410 μm internal diameter was used and 2.8 ± 0.1 Psi stable air pressure as applied for this case. The results of the printed structures are shown in Figure 2C and 2D. It was quite interesting to observe the warping of the scaffold (Figure 2D), due to dehydration. The SEM micrographs shown the surface and cross-sections morphologies of the scaffolds (Figure 2E-2M), which revealed the integrity of mesh-like structure where the adjacent layers were perpendicularly stacked to construct a rectangular porous structure. It is known that the porous structure allows sufficient oxygen and nutrient mass transport into the scaffolding system that contribute to excellent cell growth by preventing or minimizing core necrosis [18]. In addition, the intersections of adjacent layers of the filaments were tightly connected with each other, which help increasing the strength of the scaffolding system overall. It should also be noted that the current formulated hydrogel not only could be used for 3D printing of simple scaffolding system as discussed here, but also could be used to engineer complex structures. For example, various shapes and structures, including a prototype of human ear, were printed out using the A-SA-Gel hydrogel as shown in Figure 3, which further demonstrate the feasibility and printability of the hydrogel suitable for various tissue or organ engineering applications.

The chemical functional groups of albumen, SA, gelatin, and A-SA-Gel hydrogel samples were analyzed using FTIR (see Figure 4A). As seen in the spectrum, all the major characteristic peaks were observed. The FTIR spectrum of the A-SA-Gel hydrogel showed a combined the features of those of albumen, SA, and gelatin. For instance, Amid I (related to C=O stretching vibrations; the peak range of 1700–1600 cm^{-1}), amide II (related to 60% N-H bending and 40% C-H stretching vibrations; the peak range of 1575–1480 cm^{-1}), and amide III (related to N-H bending and C-H stretching vibrations; the peak range of 1400–1200 cm^{-1}) regions were clearly appeared. Moreover, the absorption band at 1021 cm^{-1} could be attributed to the C-O stretching vibration of SA [19]. From the peaks of the A-SA-Gel spectrum, it could be concluded that the mixture of albumen, SA, and gelatin did not cause any drastic alteration in the position of main peaks associated with the secondary structure of the protein present in the individual components. Moreover, it was obvious that there was no noticeable peak split was observed in the A-SA-Gel spectrum, indicating a homogeneous dispersion of albumen, SA, and gelatin.

The swelling profile curves of the A-SA-Gel and SA/Gel samples in PBS and culture medium are presented in Figure 4B and 4C, respectively. It can be seen from the graphs that the swelling patterns of all the samples were identical irrespective of the medium where the swelling experiments were carried out, and their swelling ratios increased over time during the course of the study. However,the swelling ratio of the SA/Gel sample was found to be higher than that of the A-SA-Gel sample in PBS as well as in culture medium. It was also noticed that the swelling ratio of SA/Gel and A-SA-Gel samples was rapidly increased in the first 15 minutes and then slowly stabilized. This trend indicates that the degree of deformation of the SA/Gel is higher than A-SA-Gel hydrogel, and the degree of water loss of SA/Gel is relatively higher than that of A-SA-Gel sample. Therefore, the time-dependent drying kinetics of the SA/Gel and A-SA-Gel samples were studied and the results are plotted in Figure 4D. Interestingly, as seen from the graph, the drying ratio of the SA/Gel was found to be faster than that of the A-SA-Gel. This can be attributed that the A-SA-Gel hydrogel sample has not only good hydrophilicity but also high water content which is due to the albumen's high moisturizing functional property [20]. It is noteworthy to mention that the fabrication of scaffolds that provides a moist environment is always preferable for wound healing application where it can also mainly protect the wound against microorganisms as a kind of physical barrier [21].

The results of the degradation profile of the SA/Gel and A-SA-Gel samples are given in Figure 5 along with their morphological behavior. The results show that the dissolution rate of the A-SA-Gel sample is slightly higher than that of SA/Gel. Also, it was noticed that the degradation rate of A-SA-Gel in PBS was higher than in the culture medium (see Figure 5E). This is due to the fact that the albumen protein might be involved to regulate the degradation characteristics of the A-SA-Gel hydrogel. It was also clearly noticed from the series of SEM micrographs (see Figures 5A-5B) that the morphology of the A-SA-Gel hydrogel scaffolding system became fluffy, rougher and swelling over time when compared to SA/Gel scaffolds. These results are also in accordance with swelling measurement results (Figure 4B-4C).

The suitability of hydrogels as bioinks in tissue or organ engineering often depends on their mechanical properties, and structural integrity and shape fidelity. Therefore, the mechanical properties of the formulated hydrogels were thoroughly examined. The compressive strength and the strain of A-SA-Gel hydrogel sample exceeded 6 MPa and 55%, respectively, and was higher than SA/Gel sample (see Figure 6). The data are corroborated well in accordance with earlier studies [14, 22]. As for the tensile strength, the stress and strain of A-SA-Gel hydrogel samples were higher than that of SA/Gel sample. These results clearly indicate that the 3D printed A-SA-Gel hydrogel scaffolding systems have appropriate mechanical properties and they are tunable suitable for tissue or organ-specific application.

Though the structural and mechanical properties of a scaffolding system is important for organ engineering, the cellular compatibility is the most essential property because cells are the fundamental building blocks of tissues and thus organs and they must grow well on the scaffolding system. Moreover, the scaffolds should also support the vascularization process during the tissue organization [23]. Therefore, the cellular and vascular-supportive potential of 3D printed A-SA-Gel hydrogel samples were investigated using HUVECs as a model cell. The results of the in vitro cell culture study are given in Figures 7, 8 and 9. Figure 7 clearly shows that the cells were well attached to the A-SA-Gel hydrogel substrate and were uniformly distributed throughout the scaffolding system even after 4 days of culturing. In addition, there were endothelial sprouting and the formation of branched vessel networks observed on the A-SA-Gel hydrogel scaffolds (see Figure 8), which is a good sign that the scaffolds are vascular supportive in addition to mere cell compatible. The robust neovessels were also formed; the maximum diameter and length of endothelial sprouting are found to be 112μm and 476μm, respectively.

The fluorescent stained images showed dense endothelialized layer with sprouting on the surface of the A-SA-Gel hydrogel substrate (Figure 9A-A2 and 9B-B2). In addition, the SEM micrographs also supported the claim that the HUVECs were well attached on the hydrogel substrate and spread over it (Figure 9D-9F). The CCK 8 assay data (Figure 9G) show that cells were well proliferated onto the A-SA-Gel hydrogel sample as compared to SA/Gel and Petri dish.

All these results clearly demonstrated that the 3D printed A-SA-Gel hydrogel scaffolding systems are cell compatible and vascular supportive with adequate and tunable mechanical properties. Though the SA and Gel biomaterials were widely used as a tissue scaffolding system in our earlier study, and by other groups as reported in the literature, the present study advanced the utilization of those biomaterials as self-standing and vascular supportive in 3D printing of tissue/organ scaffolding systems. The further studies are necessary; however, particularly on how the newly formulated A-SA-Gel hydrogel perform under in vivo conditions to not only to validate its in vitro results and to further examine its efficacy in tissue regeneration which is under progress and the results will be published elsewhere.

5. Conclusion

In this study, a new formulation of A-SA-Gel hydrogel was developed and tested as a self-standing and vascular supportive biomaterial suitable for 3D printing. The experimental conditions necessary for extrusion-based 3D printing of in-house formulated hydrogel with various simple to complex structures and shapes were optimized by modulating system and solution parameters. Importantly, the complex engineered structure includes a human ear model which is a realistic example of printability of our in-house formulated hydrogel. The printed hydrogel scaffolds also supported the cell growth, that is, HUVECs in this case. The cells

were proliferated well on the scaffolding system and extended to endothelial sprouting and microvascular network formation through the scaffolds during the course of the cell culture study. In overall, the in-house formulated new kind of A-SA-Gel hydrogel is a potential biomaterial that may be considered for 3D printing of tissue or organ structures.

Conflicts of interest

The authors declare that they have no conflicts of interest.

Acknowledgments

The authors acknowledge funding support from the National Natural Science Foundation of China (Grant 51775324). The authors would also like to thank the funding support from the 2019 top innovative training program of graduate students at Shanghai University (Grant Nos 2019GY04), VIT SEED grant, and research facilities of VIT.

Reference

[1] S.V. Murphy, A. Atala, 3D bioprinting of tissues and organs, Nat Biotechnol 32(8) (2014) 773-85.

[2] W. Aljohani, M.W. Ullah, X. Zhang, G. Yang, Bioprinting and its Applications in Tissue Engineering and Regenerative Medicine, International Journal of Biological Macromolecules 107(Pt A) (2017).

[3] A.G. Tabriz, M.A. Hermida, N.R. Leslie, W. Shu, Three-dimensional bioprinting of complex cell laden alginate hydrogel structures, Biofabrication 7(4) (2015) 045012.

[4] K.S. Lim, J.H. Galarraga, X. Cui, G.C.J. Lindberg, J.A. Burdick, T.B.F. Woodfield, Fundamentals and Applications of Photo-Cross-Linking in Bioprinting, Chemical Reviews 120(19) (2020) 10662-10694.

[5] B. Duan, L.A. Hockaday, K.H. Kang, J.T. Butcher, 3D Bioprinting of heterogeneous aortic valve conduits with alginate/gelatin hydrogels, J. Biomed. Mater. Res. Part A 101A(5) (2013) 1255-1264.

[6] A.L. Rutz, K.E. Hyland, A.E. Jakus, W.R. Burghardt, R.N. Shah, A Multimaterial Bioink Method for 3D Printing Tunable, Cell-Compatible Hydrogels, Advanced Materials 27(9) (2015) 1607-1614.

[7] M. Yeo, J.-S. Lee, W. Chun, G.H. Kim, An Innovative Collagen-Based Cell-Printing Method for Obtaining Human Adipose Stem Cell-Laden Structures Consisting of Core–Sheath Structures for Tissue Engineering, Biomacromolecules 17(4) (2016) 1365-1375.

[8] Y. Shin, J.S. Jeon, S. Han, G.-S. Jung, S. Shin, S.-H. Lee, R. Sudo, R.D. Kamm, S. Chung, In vitro 3D collective sprouting angiogenesis under orchestrated ANG-1 and VEGF gradients, Lab on a Chip 11(13) (2011) 2175.

[9] K.H. Song, C.B. Highley, A. Rouff, J.A. Burdick, Complex 3D-Printed Microchannels within Cell-Degradable Hydrogels, Advanced Functional Materials 28(31) (2018) 1801331.

[10] E. Bible, O. Qutachi, D.Y.S. Chau, M.R. Alexander, K.M. Shakesheff, M. Modo, Neo-vascularization of the stroke cavity by implantation of human neural stem cells on VEGF-releasing PLGA microparticles, Biomaterials 33(30) (2012) 7435-7446.

[11] K. Säljö, L.S. Orrhult, P. Apelgren, K. Markstedt, L. Kölby, P. Gatenholm, Successful engraftment, vascularization, and In vivo survival of 3D-bioprinted human lipoaspirate-derived adipose tissue, Bioprinting 17 (2020) e00065.

[12] S. Liu, H. Zhang, Q. Hu, Z. Shen, D. Rana, M. Ramalingam, Designing vascular supportive albumen-rich composite bioink for organ 3D printing, J Mech Behav Biomed Mater 104 (2020) 103642.

[13] E. Axpe, M.L. Oyen, Applications of Alginate-Based Bioinks in 3D Bioprinting, International Journal of Molecular Sciences 17(12) (2016) 1976-.

[14] S. Li, H.G. Zhang, D.D. Li, J.P. Wu, C.Y. Sun, Q.X. Hu, Characterization of Engineered Scaffolds with Spatial Prevascularized Networks for Bulk Tissue Regeneration, ACS Biomater. Sci. Eng. 3(10) (2017) 2493-2501.

[15] L. Ouyang, J.P.K. Armstrong, Y. Lin, J.P. Wojciechowski, M.M. Stevens, Expanding and optimizing 3D bioprinting capabilities using complementary network bioinks, Science Advances 6(38) (2020).

[16] G. Gao, J.H. Lee, J. Jang, D.H. Lee, J.-S. Kong, B.S. Kim, Y.-J. Choi, W.B. Jang, Y.J. Hong, S.-M. Kwon, D.-W. Cho, Tissue Engineered Bio-Blood-Vessels Constructed Using a Tissue-Specific Bioink and 3D Coaxial Cell Printing Technique: A Novel Therapy for Ischemic Disease, Advanced Functional Materials 27(33) (2017) 1700798.

[17] K. Hölzl, S. Lin, L. Tytgat, S.V. Vlierberghe, A. Ovsianikov, Bioink properties before, during and after 3D bioprinting, Biofabrication 8(3) (2016) 032002.

[18] C. Piard, H. Baker, T. Kamalitdinov, J. Fisher, Bioprinted osteon-like scaffolds enhance in vivo neovascularization, Biofabrication 11(2) (2019) 025013.

[19] Q.Q. Wang, Y. Liu, C.J. Zhang, C. Zhang, P. Zhu, Alginate/gelatin blended hydrogel fibers cross-linked by Ca(2+) and oxidized starch: Preparation and properties, Mater Sci Eng C Mater Biol Appl 99 (2019) 1469-1476.

[20] A. Jahani-Javanmardi, M. Sirousazar, Y. Shaabani, F. Kheiri, Egg white/poly (vinyl alcohol)/MMT nanocomposite hydrogels for wound dressing, J Biomater Sci Polym Ed 27(12) (2016) 1262-76.

[21] J.S. Gonzalez, L.N. Ludueña, A. Ponce, V.A. Alvarez, Poly(vinyl alcohol)/cellulose nanowhiskers nanocomposite hydrogels for potential wound dressings, Materials Science & Engineering C Materials for Biological Applications 34(1) (2014) 54-61.

[22] S.-H. Liu, H.-G. Zhang, S. Li, C.-Y. Sun, Q.-X. Hu, A Facile Strategy for Fabricating Tissue Engineering Scaffolds with Sophisticated Prevascularized Networks for Bulk Tissue Regeneration, Macromolecular Materials and Engineering (2019) 1800642.

[23] E.C. Novosel, C. Kleinhans, P.J. Kluger, Vascularization is the key challenge in tissue engineering, Advanced Drug Delivery Reviews 63(4) (2011) 300-311.

Figures for manuscript

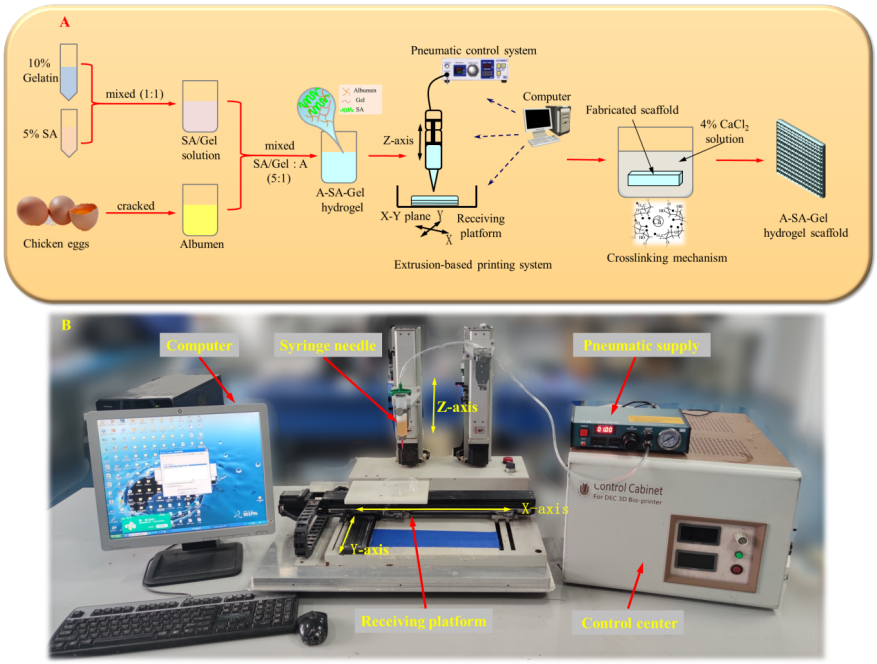

Figure 1. *(A) The schematic representation of formulation and 3D printing of* A-SA-Gel hydrogel. *(B) The in-house built extrusion-based printing system that was employed for the 3D printing of various scaffolding structures and shape from the hydrogel .*

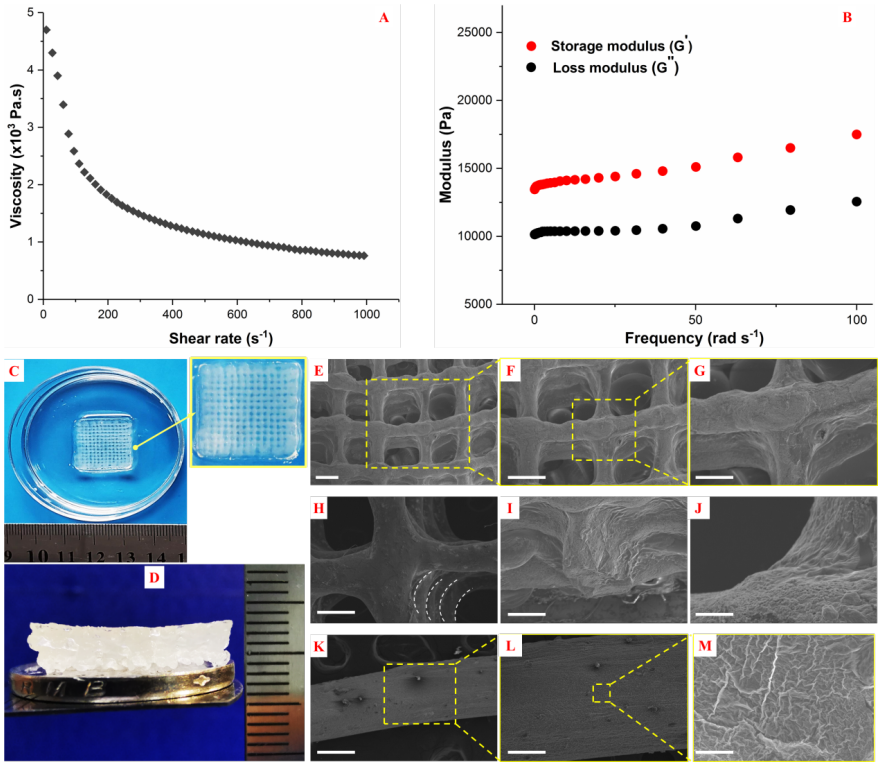

Figure 2. *Characteristics of the formulated* A-SA-Gel hydrogel *and the 3D printed scaffolds from the hydrogel: (A) The viscosity of the* hydrogel *that has a shear thinning behavior. (B) The modulus of the crosslinked* hydrogel that has *a higher storage modulus than that of loss modulus. (C-D) Photograph of the 3D printed hydrogel scaffold (top view) and its side view. (E) SEM micrographs of the top view of the printed scaffold (white dotted line indicate the different layers of the scaffolding system, σαλε βαρ: 500 μμ), (Φ-Γ) ϛορρεϛπονδινγ μαγνιφιϛατιον οφ ῎ (σϛαλε βαρ: Φ=500μμ, Γ=250μμ), (Η) τηε φιλαμεντϛ οφ διφφερεντ λαψερϛ οφ τηε σϛαφφολδ (σϛαλε βαρ:250μμ), (Ι) ϛροσσ-σεϛτιονϛ μορπηολογψ οφ τηε σϛαφφολδ (σϛαλε βαρ:250μμ), (Θ) α ϛλοσε ιεω οφ μορπηολογψ οφ τηε σϛαφφολδ (σϛαλε βαρ:50μμ), ανδ (Κ-Μ) ΣΕΜ ιμαγεϛ οφ τηε συρφαϛε οφ α σινγλε πριντεδ φιλαμεντ (σϛαλε βαρ: Κ=250 μμ,Λ=100μμ,Μ=25μμ).*

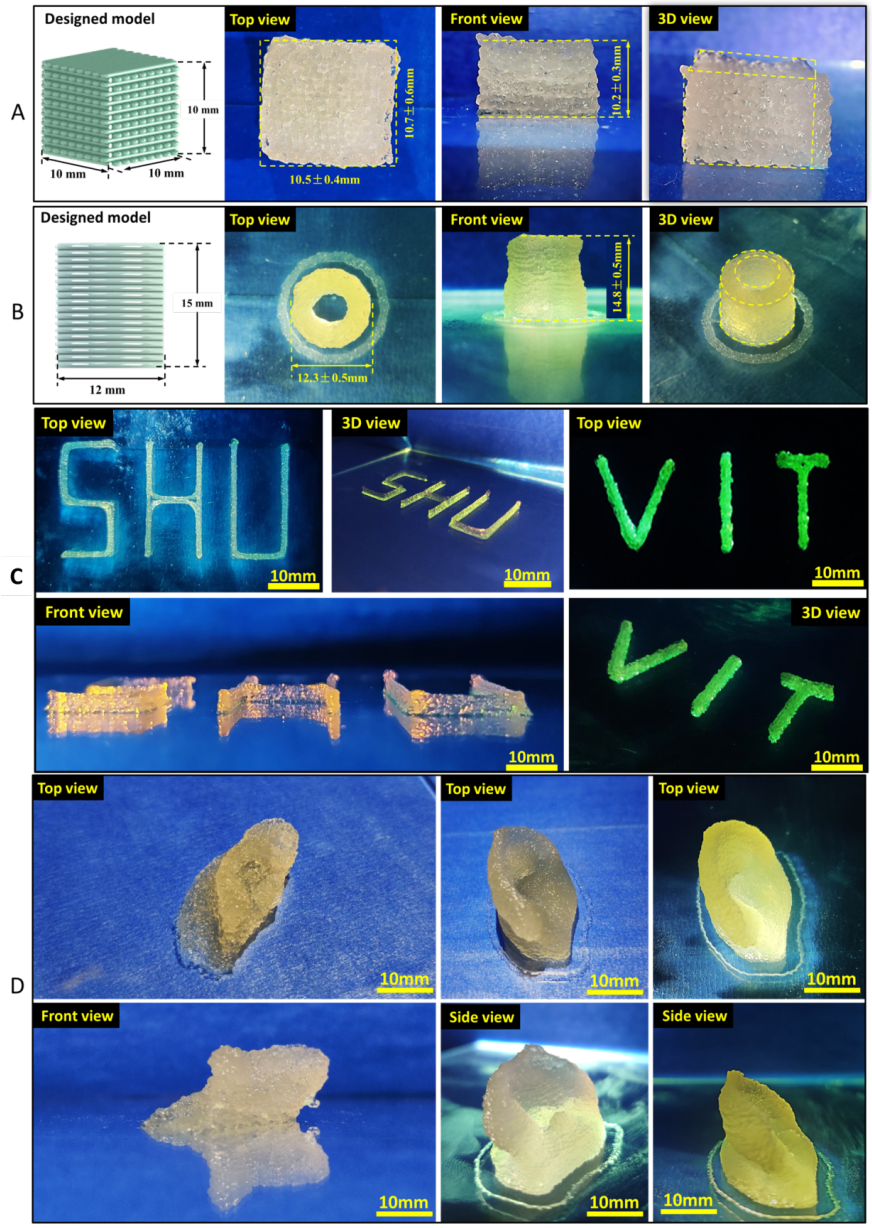

Figure 3. 3D *Printing of different structures and shapes using A-SA-Gel hydrogel: (A) 10×10×10 mm*

(L×W×H) thick scaffold structure; (B) blood vessel structure (12mm in diameter, 15mm in height); (C) the abbreviations of Shanghai University (SHU) and Vellore Institute of Technology (VIT); (D) human ear scaffold structure.

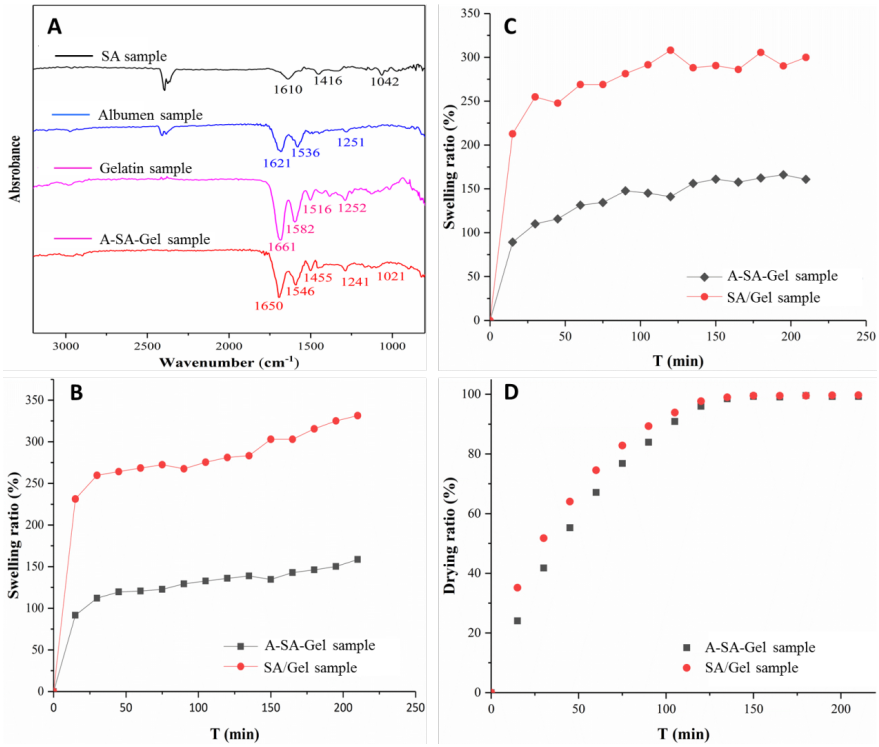

Figure 4. *(A) FTIR spectra of the SA sample, albumen sample, gelatin sample, and A-SA-Gel hydrogel sample. (B) Mass swelling ratio of A-SA-Gel hydrogel and SA/Gel samples in PBS, and the same in RPMI 1640 medium (C); (D)*

The time-dependent drying kinetics of the prepared A-SA-Gel hydrogel and SA/Gel samples at 37 °C.

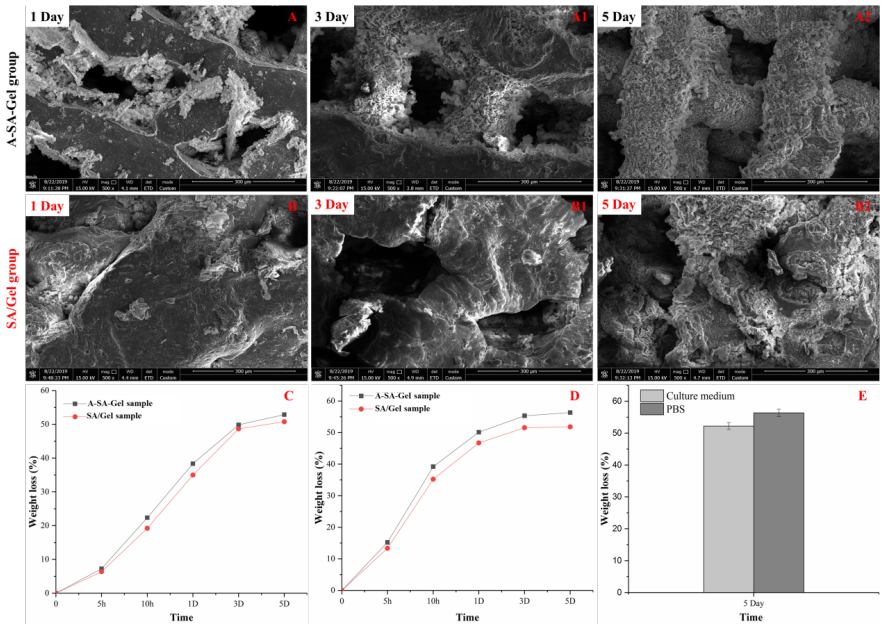

Figure 5. *The degradation behavior and the morphology after degradation of A-SA-Gel and SA/Gel hydrogel samples: (A-A2) the surface morphology of A-SA-Gel hydrogel sample after degradation of 1, 3 and 5 days; (B-B2) the surface morphology of SA/Gel hydrogel sample after degradation of 1, 3 and 5 days; (C) weight loss ratio of A-SA-Gel and SA/Gel hydrogel samples in RPMI 1640 culture medium; (D) weight loss ratio of A-SA-Gel and SA/Gel hydrogel samples in PBS; (E) weight loss ratio of A-SA-Gel and SA/Gel hydrogel samples in PBS and culture medium after degradation of 5 days.*

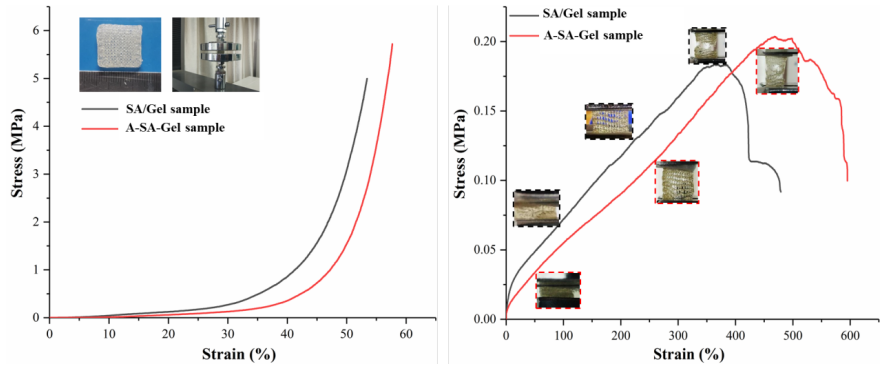

Figure 6. *Mechanical properties of the 3D printed A-SA-Gel and SA/Gel hydrogel samples: compressive strength (right) and tensile strength (left).*

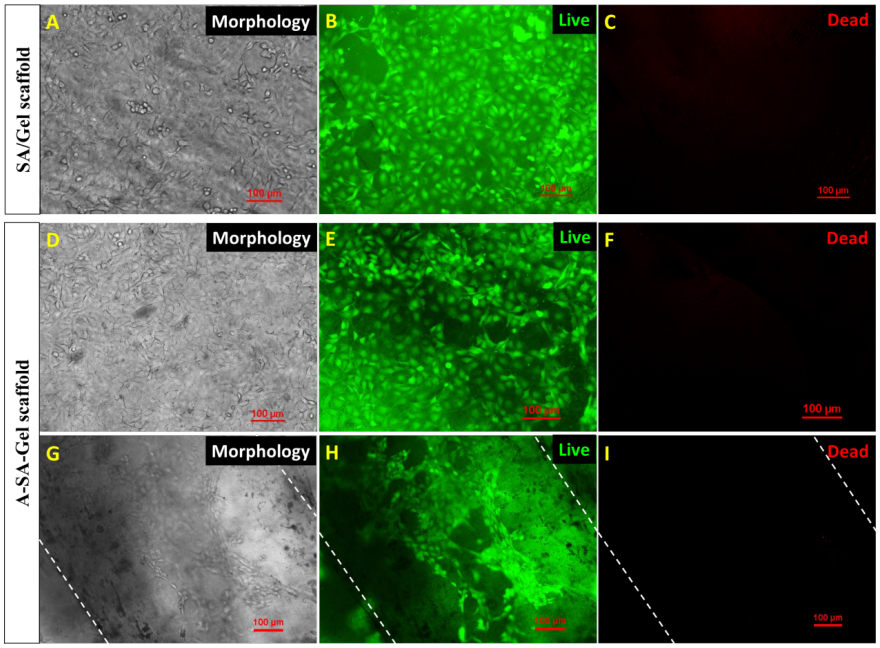

Figure 7. *Morphology and live/dead fluorescent images of the HUVECs cultured onto the SA/Gel and A-SA-Gel hydrogel scaffolds (day 4): (A-C) the SA/Gel hydrogel scaffold and (D-I) the A-SA-Gel hydrogel scaffold. White curves represent the boundaries of the filament of the scaffolding system.*

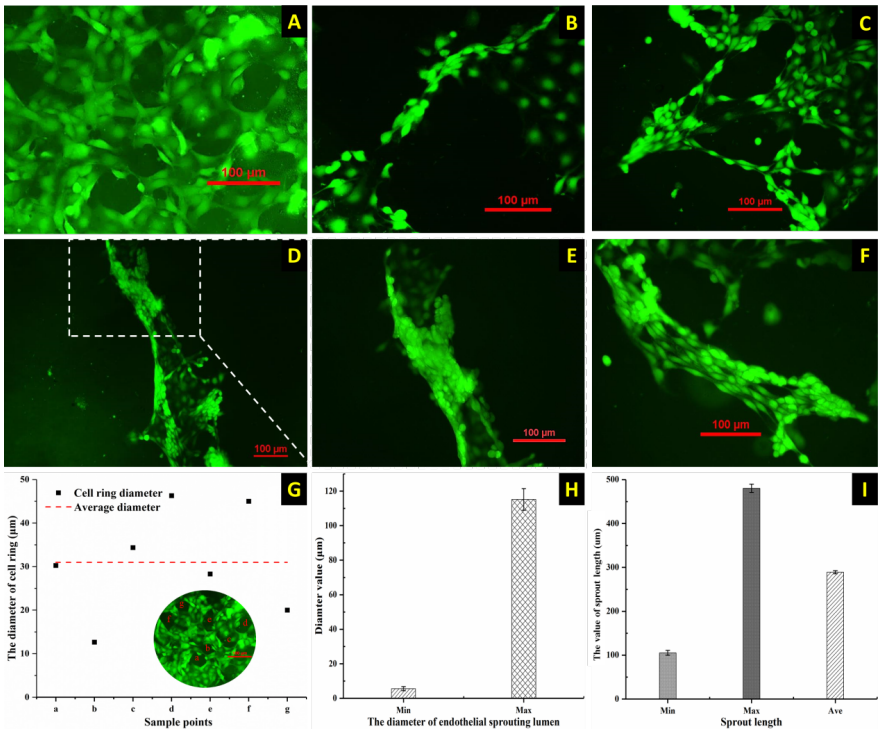

Figure 8. *The observation of endothelial sprouting cultured on the 3D printed A-SA-Gel hydrogel scaffolds after 4 days; (A-F) Fluorescent microscope images of endothelial sprouting and sprouting of neovessels*

network: (A) the formation of microvascular network, (B) a microvessel of endothelial cells like a bridge, interconnected between adjacent sides, (C) branched microvascular network, and (D-F) the formation of robust neovessels with open lumen; (G) Quantitative analysis of the diameter of endothelial cells' microvascular network; (H) Quantitative analysis of the diameter of neovessels; (I) Quantitation of the sprout length.

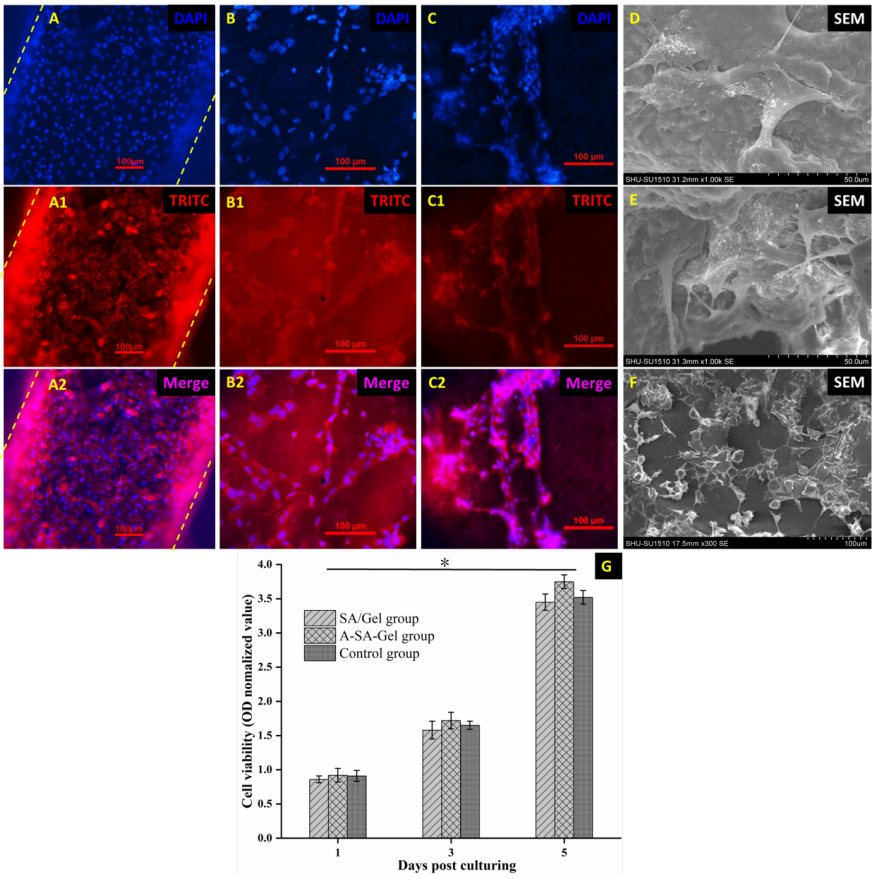

Figure 9. *Fluorescent microscopic images of cell nuclei (A-C) and cytoskeleton (A1-C1) on the surface of A-SA-Gel hydrogel scaffold after culturing 4 days; (A2-C2) the merge images of cell nuclei and cytoskeleton; (D-F) the SEM micrographs of cells attachment on the surface of A-SA-Gel hydrogel scaffold after culturing 4 days; (F) CCK-8 assay data analysis after culturing 1, 3, and 5 days. The error bars represent the standard deviation(n=6) and the value of *p [?] 0.05 was considered statistically significant.*